

Up-down asymmetry measurement of tungsten distribution in large helical device using two extreme ultraviolet (EUV) spectrometers

メタデータ	言語: eng 出版者: 公開日: 2022-01-04 キーワード (Ja): キーワード (En): 作成者: LIU, Yang, MORITA, Shigeru, Huang, Xianli, OISHI, Tetsutarou, GOTO, Motoshi, Zhang, Hongming メールアドレス: 所属:
URL	http://hdl.handle.net/10655/00012879

This work is licensed under a Creative Commons Attribution 3.0 International License.



Up-down asymmetry measurement of tungsten distribution in large helical device using two extreme ultraviolet (EUV) spectrometers

Cite as: Rev. Sci. Instrum. **87**, 11E308 (2016); <https://doi.org/10.1063/1.4959781>

Submitted: 30 May 2016 • Accepted: 27 June 2016 • Published Online: 11 November 2016

 Y. Liu, S. Morita, X. L. Huang, et al.



View Online



Export Citation



CrossMark

ARTICLES YOU MAY BE INTERESTED IN

Vertical profiles and two-dimensional distributions of carbon line emissions from C^{2+} – C^{5+} ions in attached and RMP-assisted detached plasmas of large helical device

Physics of Plasmas **24**, 022510 (2017); <https://doi.org/10.1063/1.4976989>

Effect of neutron and γ -ray on charge-coupled device for vacuum/extreme ultraviolet spectroscopy in deuterium discharges of large helical device

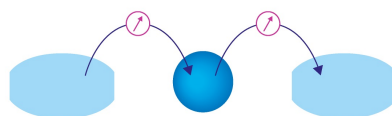
Review of Scientific Instruments **89**, 101109 (2018); <https://doi.org/10.1063/1.5037233>

Pioneering work before becoming mainstream research

AIP Conference Proceedings **1993**, 020001 (2018); <https://doi.org/10.1063/1.5048711>

Webinar

Interfaces: how they make or break a nanodevice



March 29th – Register now



Zurich
Instruments



Up-down asymmetry measurement of tungsten distribution in large helical device using two extreme ultraviolet (EUV) spectrometers

Y. Liu,^{1,a)} S. Morita,^{1,2} X. L. Huang,² T. Oishi,^{1,2} M. Goto,^{1,2} and H. M. Zhang¹

¹Department of Fusion Science, Graduate University for Advanced Studies, Toki, Gifu 509-5292, Japan

²National Institute for Fusion Science, Toki, Gifu 509-5292, Japan

(Presented 8 June 2016; received 30 May 2016; accepted 27 June 2016;
published online 2 August 2016)

Two space-resolved extreme ultraviolet spectrometers working in wavelength ranges of 10–130 Å and 30–500 Å have been utilized to observe the full vertical profile of tungsten line emissions by simultaneously measuring upper- and lower-half plasmas of LHD, respectively. The radial profile of local emissivity is reconstructed from the measured vertical profile in the overlapped wavelength range of 30–130 Å and the up-down asymmetry is examined against the local emissivity profiles of WXXVIII in the unresolved transition array spectrum. The result shows a nearly symmetric profile, suggesting a good availability in the present diagnostic method for the impurity asymmetry study. *Published by AIP Publishing.* [<http://dx.doi.org/10.1063/1.4959781>]

I. INTRODUCTION

In the next-generation fusion device, ITER (International Thermonuclear Experimental Reactor), the material of plasma-facing components must have good capability of tolerating extremely large thermal heat load, in addition to lower erosion and tritium retention rates. For this reason, the tungsten is scheduled to be used in the ITER instead of carbon material.^{1,2} Study on the tungsten transport is therefore important for suppressing the impurity accumulation at the plasma core and enhancing the impurity screening at the plasma edge. Until now the impurity transport has been basically studied as a function of the magnetic surface. In high-Z impurities such as tungsten, however, the radial distribution often shows an asymmetric profile. Up-down and in-out asymmetries for argon, nickel, tungsten, etc., are reported in JET³ and Alcator C-mod.⁴ Both the neoclassical⁵ and anomalous radial transports⁶ have been proved to be sensitive to the asymmetric profile formation. The strong poloidal asymmetry can lead to the misinterpretation of measured data, if the full profile is not obtained in the experiment.

The tungsten transport study has been recently started in LHD using tungsten pellet injection. Full vertical profiles of tungsten line emissions have been successfully observed at upper- and lower-half plasma radii based on the simultaneous measurement using two space-resolved extreme ultraviolet (EUV) spectrometers. In order to check the availability of the present diagnostic method for impurity asymmetry study, the radial profiles of local emissivity after Abel inversion is compared in the upper- and lower-half plasmas and the up-down asymmetry is then examined for WXXVIII emission.

II. EXPERIMENTAL SET-UP

Two space-resolved EUV spectrometers, EUV_Long2⁷ and EUV_Short2,⁸ are installed on the #10-O port in LHD for measuring the spatial distribution of impurity line emissions in the wavelength ranges of 30–500 Å and 10–130 Å, respectively. The LHD plasma at the port center is horizontally elongated with vertical diameter of $\Delta Z = \sim 1.0$ m including the stochastic magnetic field layer. A schematic diagram of two spectrometer arrangements is shown in Fig. 1. The cubic vacuum chamber shared by two spectrometers is evacuated by a magnetically floating turbo molecular pump and is kept in the order of 10^{-8} Torr. The optical axes of both spectrometers are perpendicular to the magnetic axis. The 1.2 m long toroidal slit with comb-like rectangular-corrugated apertures installed in the vacuum chamber 3 m away from the spectrometers is used to calibrate the elevation angle of each observation chord. Both spectrometers have identical structures except for the number of grooves and angle of incidence of the grating, i.e., an entrance slit, a spatial resolution slit placed in front of the entrance slit, a gold-coated concave varied-lines-spacing (VLS) laminar-type holographic grating, and a back-illuminated charge-coupled device (CCD) detector. The VLS grating with 1200 (2400) grooves/mm for EUV_Long2 (EUV_Short2) covers the wavelength range of 30–500 Å (10–130 Å). Since a relatively long distance is required between the spectrometer and the plasma to observe a wider vertical plasma range, e.g., 0.5 m, which corresponds to half diameter at the short axis of the elliptical LHD plasma, the spectrometers have to be placed at a long distance of 9452 mm from the plasma center to the spectrometer entrance slit. The large distance leads to a large multiplication factor, which slightly depends on the spectral wavelength, e.g., 19.98 at CVI 33.74 Å and 19.65 at HeII 303.78 Å. The CCD is cooled down to -20° by a Peltier device to reduce the thermal noise. The CCD has an effective area of 26.6×6.6 mm² with the total number of pixels of 1024×255 (26×26 μm^2 /pixel). The vertical profile and the spectrum are then recorded along the CCD long and

Note: Contributed paper, published as part of the Proceedings of the 21st Topical Conference on High-Temperature Plasma Diagnostics, Madison, Wisconsin, USA, June 2016.

^{a)}Author to whom correspondence should be addressed. Electronic mail: liu.yang@nifs.ac.jp

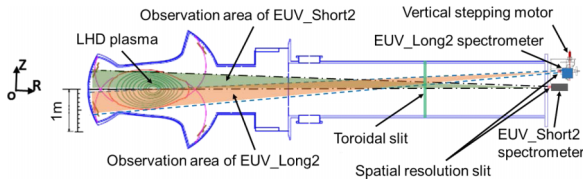


FIG. 1. Side view of two space-resolved EUV spectrometers.

short axes, respectively. The CCD detector is operated in two readout modes of full resolution image and sub-image. The full resolution image mode which can yield experimental data with the best spectral resolution is used only for the spectral resolution test and the line identification because the necessary exposure time is very long. The sub-image mode is used for the routine measurement on the impurity profile. One kind of sub-images with 127×204 channels is usually used by summing up two adjacent pixels in the short axis and five adjacent pixels in the long axis. Thus, the spectra of impurity emissions are obtained with exposure time of 61.5 ms and sampling time of 100 ms. The spectral intensity measured by the EUV spectrometers is absolutely calibrated on the basis of simultaneous profile measurement of bremsstrahlung continua in the EUV and visible ranges. The vertical observation range of EUV_Short2 is fixed to the upper half plasma observation ($0 \leq Z \leq 50$ cm). In contrast, the vertical observation range of EUV_Long2 ($\Delta Z \sim 53$ cm) can be freely selected by changing the vertical angle of the spectrometer optical axis. But the vertical angle change may create a systematic error in the absolute position of observation chords. The absolute position of observation chords in EUV_Short2 seems to be more accurate than that in EUV_Long2. Therefore, the vertical position calibration is frequently required for EUV_Long2 to accurately analyze the profile data.

In the present study, EUV_Long2 for lower-half observation is combined with EUV_Short2 for upper-half observation to provide the full vertical profile of tungsten emission lines in the overlapped wavelength range of 30-130 Å. In general LHD plasma discharges, CVI (33.73 Å) intensity is strong enough for the accurate positional calibration of all observation chords. Then, the positional calibration is carried out with the CVI vertical profile assuming that the CVI locates at the same radial position in both the upper- and lower-half plasmas. Thus, the up-down asymmetry study is possible for tungsten.

III. EXPERIMENTAL RESULTS

A series of experiments on the high-Z impurity study have been done in LHD by injecting an impurity pellet. EUV spectra from tungsten ions in high-ionization stages have been observed in LHD. A typical discharge with a relatively big coaxial tungsten pellet (tungsten wire: 0.05 mm in diameter \times 0.7 mm in length, graphite cylinder: 0.7 mm in diameter \times 0.7 mm in length) injected at the horizontal mid-plane is shown in Fig. 2. The discharge is maintained by two negative-ion-source-based neutral beams (n-NBI#1 and #2) with energy of 180 keV during 4.7-5.7 s and by two positive-ion-source-based neutral beams (p-NBI#4 and

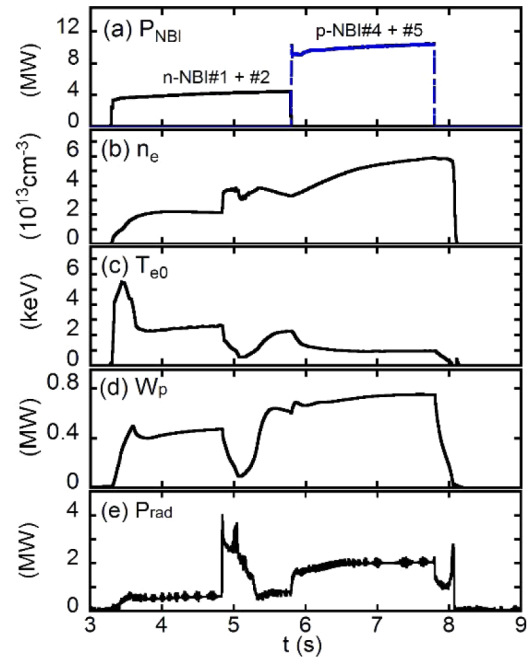
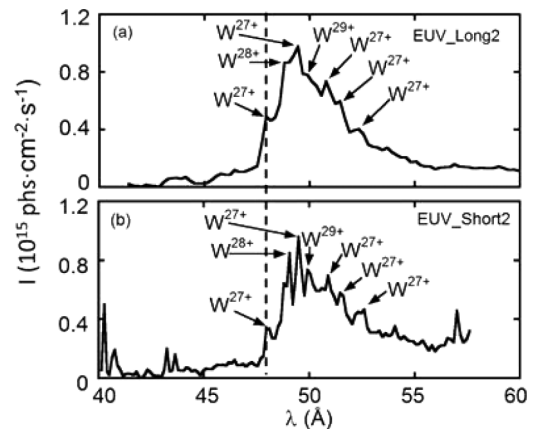


FIG. 2. Discharge waveform with tungsten pellet injection at 4.8 s: (a) NBI port-through power, (b) line-averaged electron density, (c) central electron temperature, (d) plasma stored energy, and (e) total radiation power.

#5) with energy of 40 keV. Line-averaged electron density, n_e , quickly increases at pellet injection of $t = 4.8$ s. It also gradually increases during p-NBI phase due to the reduction of edge particle screening. Central electron temperature, T_{e0} , and plasma stored energy, W_p , rapidly decrease and then slowly recover during the n-NBI phase. Radiation power after rapid increase gradually decreases and reaches the original level after 0.5 s of the pellet injection.

The unresolved transition array (UTA) spectra from tungsten ions measured at 5.3 s are shown for EUV_Long2 and EUV_Short2 in Fig. 3 with the wavelength range of 40-60 Å, while the observed ranges of EUV_Long2 and EUV_Short2 are 41-70 Å and 40-57 Å, respectively. The tungsten ionization stages are also denoted in the figures with arrows. It should

FIG. 3. Tungsten UTA spectra at $t = 5.3$ s measured with (a) EUV_Long2 and (b) EUV_Short2. It should be noticed that the apparent spectral resolution is not good in both the EUV_Long2 and EUV_Short2 because the binning is made in the CCD horizontal pixel for faster sampling time.

be noted here that the tungsten ions seen in the UTA spectra are located in the plasma center at $t = 5.3$ s and the centrally peaked emission profile can give more accurate analysis on the up-down asymmetry. The identification is done with the EUV spectra measured by a high-time response EUV_Short spectrometer without spatial resolution.⁹ It is noted here that the spectral resolution of EUV_Short is considerably high in this wavelength range compared to EUV_Long,¹⁰ as shown in Fig. 3. UTA spectra usually appeared in the electron temperature range of 1-2 keV at the wavelength interval of 45-70 Å. Since the UTA consists of many transitions from tungsten ions in different ionization stages and the spectral lines overlap each other, it is often difficult to extract an emission line.

The vertical profiles at 5.3 s (0.5 s after tungsten pellet injection) extracted from the single channel near 48 Å are plotted in Fig. 4. The ionization stage of tungsten at the wavelength is believed to be W^{27+} ions. The lower-half profile in Fig. 4(a) is taken from EUV_Long2 data at the wavelength interval of $48.04 \text{ Å} \leq \lambda \leq 48.26 \text{ Å}$ and the upper-half profile is taken from EUV_Short2 data at the wavelength interval of $48.03 \text{ Å} \leq \lambda \leq 48.16 \text{ Å}$. In order to extract the wavelength interval shown in Fig. 4(a), we have carefully checked the vertical profiles in the whole wavelength range of UTA shown in Fig. 3. In several profiles at different wavelengths in the UTA, the second peak appears in addition to the central peak indicating certain tungsten emission from lower ionization

stages is blended. Such data are avoided from the present analysis.

In order to examine the apparent up-down asymmetry, the lower-half profile is superimposed on the upper-half profile. The result is shown in Fig. 4(b). It is understood that the two vertical profiles almost overlap each other at every vertical position, suggesting no asymmetry obviously exists. Due to a different arrangement of EUV_Long2 and EUV_Short2 shown in Fig. 1, the observation chord length and angle in plasmas are slightly different between EUV_Long2 and EUV_Short2. The effect of different arrangements on the asymmetry study may not be negligible. Therefore, the up-down asymmetry is also examined against the local emissivity profile.

The radial profile of local emissivity is analyzed by reconstructing the measured vertical profile based on the Abel inversion method in which the magnetic surface necessary for the analysis is calculated with VMEC code. The lower- and upper-half vertical profiles are separately analyzed based on the data in Fig. 4 taking into account the wavelength-dependent intensity calibration factor for both the spectrometers. Since a relatively large spike noise appears in the vertical profile from EUV_Short2, which is caused by the high-energy neutrals originating in NBI fast ions, a polynomial fitting is applied in analyzing the vertical profile. A series of intersections are obtained based on the observation chords and the magnetic surfaces calculated with VMEC code, and the unit chord length between two adjacent magnetic surfaces is then calculated for all the observation chords. The local emissivity, $\varepsilon(\rho)$, is then obtained by the following equation:

$$I(r) = \Sigma \varepsilon(\rho) \Delta l, \quad (1)$$

where $I(r)$ and Δl represent the emission intensity in the vertical profile and unit chord length, respectively. The local lower- and upper-half emissivity profiles analyzed for the WXXVIII emission are plotted in Fig. 5. It also shows the same result as shown in Fig. 4(b). No significant difference showing the asymmetry is found at least in the present experimental condition. It is then understood that the effect of different arrangements between the two spectrometers is entirely small.

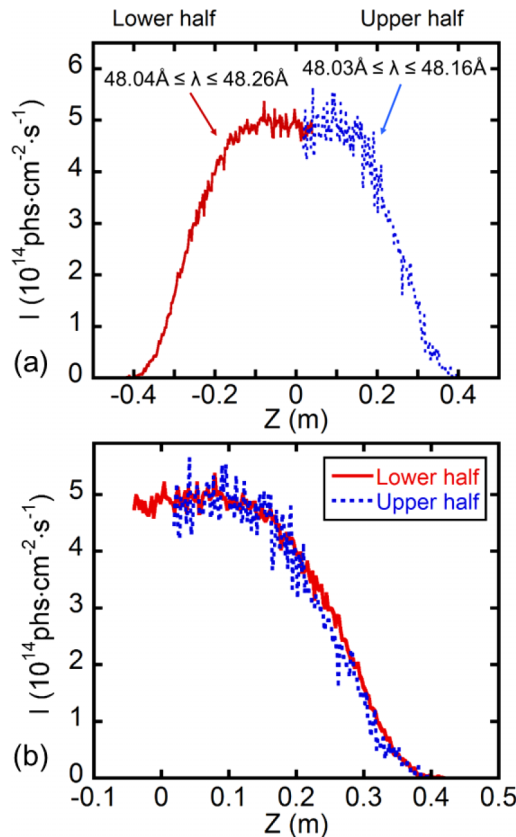


FIG. 4. (a) Vertical profiles of WXXVIII at lower- (solid line) and upper-half (dashed line) plasma radii at $t = 5.3$ s measured with EUV_Long2 and EUV_Short2, respectively, and (b) lower-half profile superimposed on the upper-half profile.

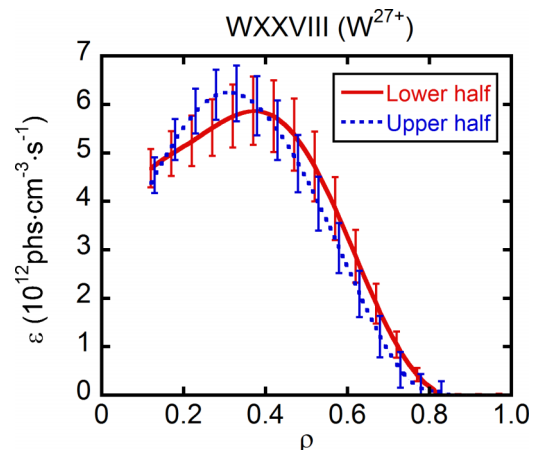


FIG. 5. Local emissivity profiles of WXXVIII at lower- (solid line) and upper-half (dashed line) plasma radii reconstructed with the Abel inversion method.

In summary, the emissivity profile of tungsten ions is symmetric within the data uncertainty at the present discharge condition. It should be also mentioned that the present method of utilizing two space-resolved EUV spectrometers to simultaneously observe the full vertical profile can work well for the asymmetry study of heavier impurity ions.

ACKNOWLEDGMENTS

The authors thank all the members of the LHD experiment group for their cooperation including technical supports. This work was partly supported by LHD project

(NIFS16ULPP010), Grant-in-Aid for Scientific Research (B) No. 16H04088 and the JSPS-NRF-NSFC A3 Foresight Program in the field of Plasma Physics (NSFC: No.11261140328 and NRF: No. 2012K2A2A6000443).

¹G. F. Matthews *et al.*, *Phys. Scr.* **T128**, 137 (2007).

²R. A. Pitts *et al.*, *Phys. Scr.* **T138**, 014001 (2009).

³L. C. Ingesson *et al.*, *Plasma Phys. Controlled Fusion* **42**, 161 (2000).

⁴K. D. Marr *et al.*, *Plasma Phys. Controlled Fusion* **52**, 055010 (2010).

⁵K. Indireskumar *et al.*, *Phys. Fluids B* **5**, 1850 (1993).

⁶T. Fulop *et al.*, *Phys. Plasmas* **18**, 030703 (2011).

⁷C. F. Dong *et al.*, *Rev. Sci. Instrum.* **81**, 033107 (2010).

⁸X. Huang *et al.*, *Rev. Sci. Instrum.* **85**, 043511 (2014).

⁹M. B. Chowdhuri *et al.*, *Appl. Opt.* **47**, 135–146 (2008).

¹⁰M. B. Chowdhuri *et al.*, *Rev. Sci. Instrum.* **78**, 023501 (2007).